KLOE Note n. 182

January 2003

Measurement of the ratio $\Gamma(K_L \to \gamma\gamma)/\Gamma(K_L \to \pi^0\pi^0\pi^0)$

S. Di Falco [a], G. Lanfranchi [b], E. Santovetti [c]

[a] Dipartimento di Fisica dell'Università e Sezione INFN, Pisa
[b] Laboratori Nazionali di Frascati dell'INFN, Frascati
[b] Dipartimento di Fisica dell'Università e Sezione INFN, Roma II

March 28, 2003

Abstract

A measurement of the ratio $R = \Gamma(K_L \to \gamma\gamma)/\Gamma(K_L \to \pi^0\pi^0\pi^0)$ with 1% accuracy is presented, based on 362 pb^{-1} integrated luminosity collected during 2001 and 2002. The measured value $R = (2.79 \pm 0.02_{stat} \pm 0.02_{syst}) \times 10^{-3}$ is in excellent agreement with the recent NA48 result. The K_L tagging procedure, neutral vertex measurement, evaluation of the selection efficiencies and background are presented. The contributions to the systematic error are discussed.

1 Introduction

The measurement of $\Gamma(K_L \to \gamma\gamma)$ is a good test of Chiral Perturbation Theory and provides useful information to put constraints on the value of the ρ parameter of the CKM matrix from the existing measurement of $\Gamma(K_L \to \mu^+\mu^-)$. For results see reference [1].

A recent measurement of the NA48 collaboration [2] gives $\Gamma(K_L \to \gamma\gamma)/\Gamma(K_L \to \pi^0\pi^0\pi^0) = (2.81 \pm 0.01_{stat} \pm 0.02_{syst}) \times 10^{-3}$. The same ratio has been measured with the 2001 and 2002 KLOE data sample corresponding to an integrated luminosity of 362 pb^{-1}, 141 pb^{-1} collected in 2001 and 221 pb^{-1} in 2002.

1.1 Method of the measurement

The $K_L \to \pi^0\pi^0\pi^0$ and $K_L \to \gamma\gamma$ events are tagged using $K_S \to \pi^+\pi^-$ decays and are identified by the reconstruction of a neutral vertex inside a given fiducial volume, FV. The ratio R can be written as $R = N_{\gamma\gamma}/N_{\pi^0\pi^0\pi^0}$ with

$$N = \frac{N_{obs} - N_{bkg}}{\epsilon_{trigger} \cdot \epsilon_{filfo} \cdot \epsilon_{tag} \cdot \epsilon_{FV} \cdot \epsilon_{sel}}$$

N_{obs} and N_{bkg} are the numbers of observed and background events for the two decay channels; $\epsilon_{trigger}$, ϵ_{filfo}, ϵ_{tag}, ϵ_{FV} and ϵ_{sel} are respectively the trigger efficiency, the FILFO filter efficiency, the tagging efficiency, the FV acceptance and the selection efficiencies for the two decays. In the measurement of R, ϵ_{tag} cancels and $\epsilon_{trigger}$ and ϵ_{filfo} are expected within few per mil, whereas background subtraction and selection efficiencies must be evaluated and brought to the same level of accuracy.

2 The neutral vertex reconstruction

The neutral vertex reconstruction for $K_L \to \pi^0\pi^0\pi^0$ is the standard one performed in the event classification [3]. We recall the *time of flight triangle* (Fig. 1) for deriving the equations for the unknown K_L decay path L_K:

$$\begin{aligned} L^2 + L_K^2 - 2LL_K\cos\theta &= L_\gamma^2 \\ L_K/\beta + L_\gamma &= ct_\gamma \end{aligned}$$

where t_γ is the cluster time at the shower centroid, $\beta_K c$ is the K_L velocity derived from the K_L momentum ($\vec{p}_{K_L} = \vec{p}_\phi - \vec{p}_{K_S}$), L_γ is the distance travelled by the photon, L is the distance from the ϕ vertex to the cluster centroid and θ is the angle between the K_L direction and the line connecting the ϕ vertex and the cluster centroid. The value of L_K is obtained from the energy weighted average:

$$L_K = \frac{\sum_i E_i \cdot l_{Ki}}{\sum_i E_i}$$

where $i = 1, ...N$ with N the number of selected clusters. The reliability of this method has been proven with a $K_S \to \pi^+\pi^- \times K_L \to \pi^+\pi^-\pi^0$ sample, making the difference between the K_L decay path reconstructed by the drift chamber from the two charged tracks (L_K^{DC}) and the K_L path reconstructed from the two photons using the time of flight triangle (L_K^{EMC}).

The result is shown in Fig. 2. The difference between the two independent measurements is constant over all the fiducial volume and shows a residual offset of 5 mm.

The accuracy on the L_K measurement is given by the dispersion of the residuals distribution obtained by making the difference between the K_L decay path l_n^{th}, evaluated with the n^{th} photon, with respect to the average $< L_K^{n-1} >$ obtained from the others $n-1$ photons (Fig. 3).

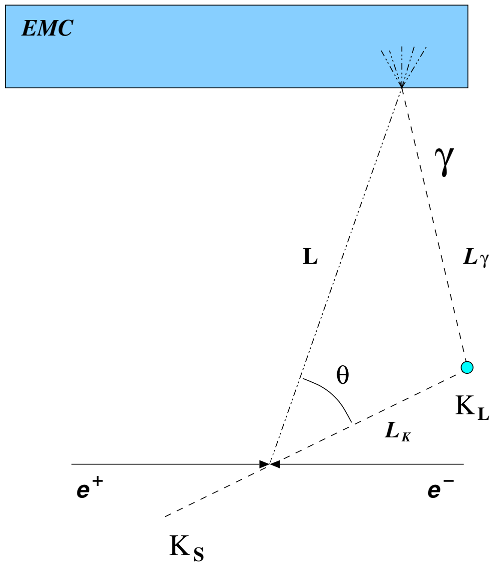

Figure 1: The time of flight triangle.

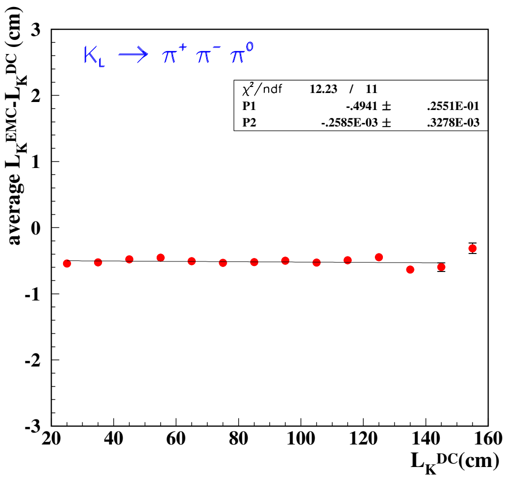

Figure 2: Difference between the K_L decay path reconstructed by the drift chamber from the two charged tracks (L_K^{DC}) and the K_L path reconstructed from the two photons using the time of flight triangle (L_K^{EMC}) for a $K_L \to \pi^+\pi^- \pi^0$ data sample as a function of L_K^{DC}.

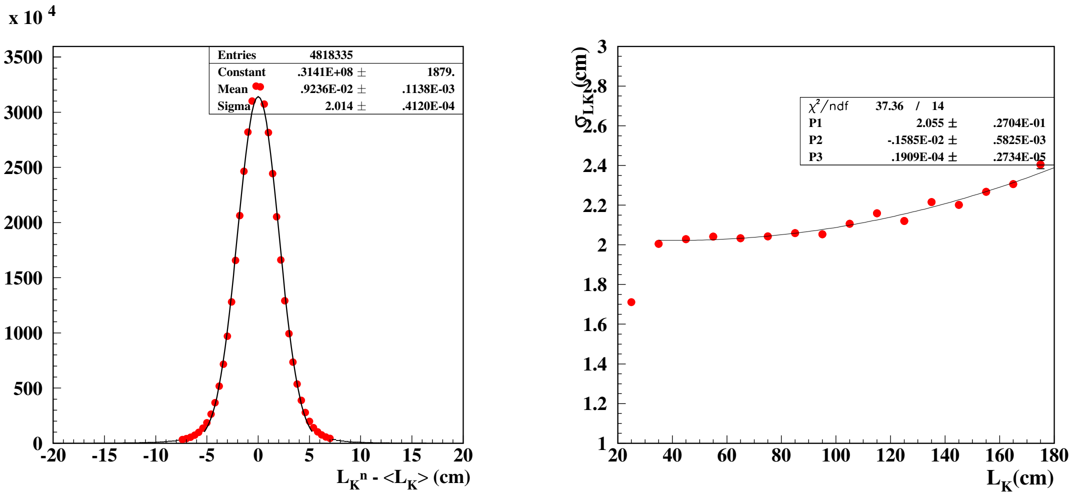

Figure 3: Dispersion of the residuals distribution of L_K measurement for $K_L \to \pi^0\pi^0\pi^0$ events: inclusive (left) and as a function of L_K (right). In the second plot the curve has been fitted with $f(L_K) = p_1 + p_2 \cdot L_K + p_3 \cdot L_K^2$.

2.1 The fiducial volume

The K_L fiducial volume (FV) is defined as:

$$30 \text{ cm} \leq r_t \leq 170 \text{ cm} \qquad |z| \leq 140 \text{ cm}$$

The corresponding acceptance is evaluated with Monte Carlo and is $\epsilon_{acc} = (31.5 \pm 0.1)\%$. The external boundary is chosen to keep the K_L decay vertex far from the calorimeter surface to reduce the overlaps between the photon clusters. The inner boundary is chosen to avoid the regeneration of the K_L in the beam pipe and the inner wall of the drift chamber. Fig. 4 shows the boundaries of the fiducial volume.

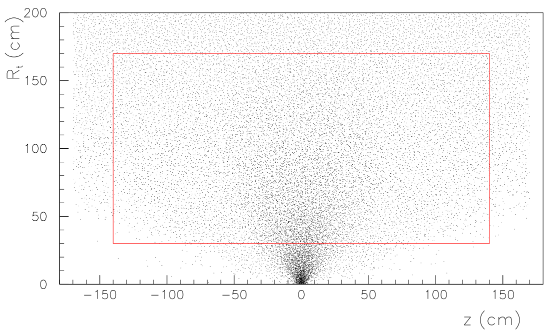

Figure 4: Fiducial Volume for K_L decays.

3 The K_L tag

3.1 The standard KLTAG

The K_L is tagged using the $K_S \to \pi^+\pi^-$ decay. The standard KLTAG algorithm requires:

1. a single reconstructed vertex inside the K_S fiducial volume defined as:

$$r_t \leq 4 \text{ cm} \qquad |z| \leq 8 \text{ cm}$$

2. two and only two tracks with opposite charge connected to the vertex;

3. p_{K_S} in the ϕ rest frame and M_{K_S} in the range:

$$50 \text{ MeV} \leq p_{K_S} \leq 170 \text{ MeV} \qquad 400 \text{ MeV} \leq M_{K_S} \leq 600 \text{ MeV}$$

These cuts are quite loose, in order to have very high efficiency compatible with a very small background. The contamination in the tagged sample due to other ϕ decays ($\phi \to K^+K^-$ or $\phi \to K_S K_L$ with $K_S \to \pi^0\pi^0$ and $K_L \to \pi^+\pi^-\pi^0$ or $K_L \to \pi\mu\nu, \pi e\nu$) and Bhabha scattering events has been estimated with Monte Carlo to be $\sim 1\%$ [4]. The contamination in the data can be estimated from the tails in the p_{K_S} and M_{K_S} distributions when normalized to the same number of Monte Carlo events. Fig. 5 shows that the contamination is at few per cent level.

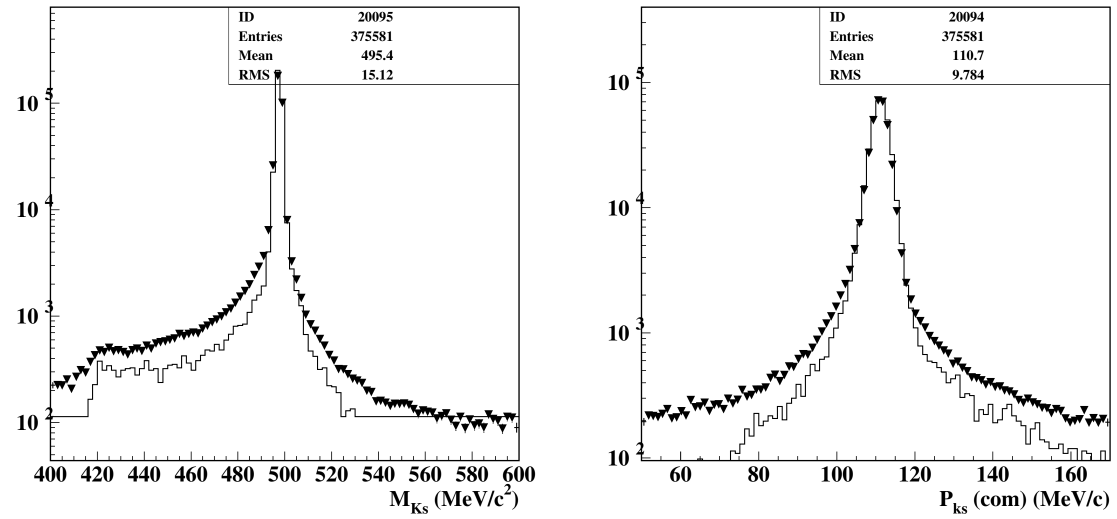

Figure 5: Invariant mass and total momentum for the tracks selected by the KLTAG algorithm. The difference between the dots (data) and the continuous line (Monte Carlo) in the tails of the distribution gives an estimate of the background.

The accuracy in the determination of the K_L direction, reconstructed from the momentum of the K_S and of the ϕ, can be evaluated using the position of the $\pi^+\pi^-$ vertex in $K_L \to \pi^+\pi^-\pi^0$ decays: the direction of the K_L is reconstructed with an accuracy of $1.7°$ in the azimuthal angle and $2.0°$ in the polar angle (Fig. 6).

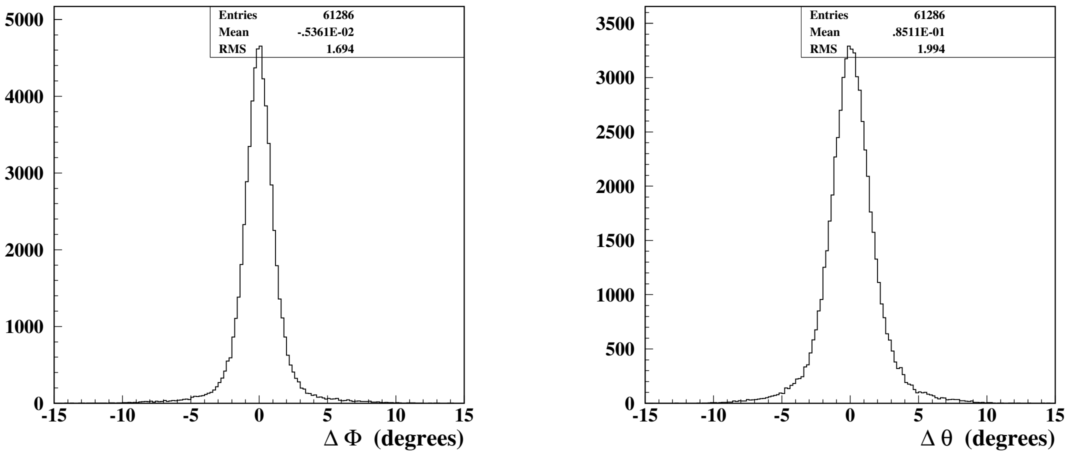

Figure 6: Distribution of the difference on the azimuth (left) and on the polar angle (right) of the K_L direction reconstructed from K_S and ϕ momentum with respect to the one estimated from the position of $\pi^+\pi^-$ vertex in $K_L \to \pi^+\pi^-\pi^0$ events.

The KLTAG algorithm efficiency (Table 1) estimated with Monte Carlo shows an evident dependence on the K_L decay channel; in particular for the charged decay channels the efficiency gets worse when the average track momentum decreases. For the K_L neutral decays, instead, this efficiency is the same within errors so that it cancels in the $(K_L \to \gamma\gamma)/(K_L \to \pi^0\pi^0\pi^0)$ ratio.

K_L channel	efficiency
$K_L \to \pi^0\pi^0\pi^0$	79.2 $\pm$ 0.2 %
$K_L \to \pi^0\pi^0$	79.1 $\pm$ 0.2 %
$K_L \to \gamma\gamma$	79.1 $\pm$ 0.2 %
$K_L \to \pi^+\pi^-$	76.7 $\pm$ 0.2 %
$K_L \to \pi e\nu$	75.7 $\pm$ 0.3 %
$K_L \to \pi\mu\nu$	75.7 $\pm$ 0.3 %
$K_L \to \pi^+\pi^-\pi^0$	73.6 $\pm$ 0.4 %
K_L on calorimeter	79.3 $\pm$ 0.2 %

Table 1: Monte Carlo KLTAG efficiencies for different K_L decays.

3.2 The restricted KLTAG

For neutral K_L decays, the $K_S \to \pi^+\pi^-$ decay must provide not only the tag but also the K_L direction and the absolute time of the event, t_0. A good resolution on the K_L direction and the exact determination of the absolute time of the event are required in order to guarantee an homogeneous reconstruction of the $K_L \to \pi^0\pi^0\pi^0$ and $K_L \to \gamma\gamma$ samples. For this reasons a restricted KLTAG algorithm has been implemented. The kinematic cuts have been restricted to:

$$100\ \text{MeV} \le p_{K_S} \le 120\ \text{MeV} \qquad 490\ \text{MeV} \le M_{K_S} \le 505\ \text{MeV}$$

The efficiency of these cuts, evaluated with Monte Carlo, is $\epsilon_{kin} = (92.1 \pm 0.1)\%$. The accuracy in the determination of the K_L direction after the kinematic cuts on the K_S invariant mass and momentum is shown in Fig. 7: the direction of the K_L is reconstructed with an resolution of $\Delta\phi = 1.5°$ and $\Delta\theta = 1.8°$.

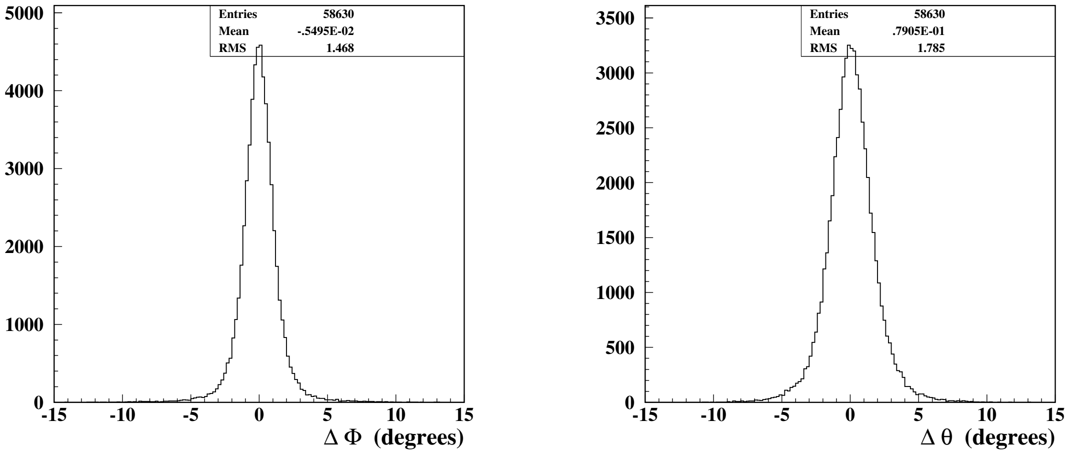

Figure 7: Distribution of the difference on the azimuth (left) and on the polar angle (right) of the K_L direction reconstructed from K_S and ϕ momentum with respect to the one estimated from the position of $\pi^+\pi^-$ vertex in $K_L \to \pi^+\pi^-\pi^0$ events after the restricted kinematic cuts on the K_S invariant mass and momentum.

3.3 The bunch crossing determination

The determination of the absolute time of the event (i.e. the identification of the bunch crossing) is crucial in the neutral vertex reconstruction both for $K_L \to \gamma\gamma$ and $K_L \to \pi^0\pi^0\pi^0$ events. When a KLTAG occurs, a correction to the first determination of the event t_0 is obtained comparing the time measured by the calorimeter $t^0_{measured}$ for one of the two pions [1] with the expected time evaluated from the corresponding track length:

$$\begin{aligned} \Delta t &= t^0_{measured} - t_{expected} = \\ &= t^0_{measured} - (L_{vtx} + L_{track} + L_{tclo} + L_{ac})/\beta_\pi c \end{aligned}$$

where L_{vtx} is the track length from the decay vertex to the first hit in the chamber, L_{track} is the track length from the first to the last hit, L_{tclo} is the extrapolation of the track from the last hit to the calorimeter surface and L_{ac} is the distance from the calorimeter surface to the cluster centroid.

A track is associated to a calorimeter cluster if the distance between the position of the cluster centroid and the extrapolation of the track, normalized to the resolution of the calorimeter in the coordinate along the fiber direction, $\sigma_z(\mathrm{E}) \sim 1\ \mathrm{cm}/\sqrt{\mathrm{E(GeV)}}$, is less than 10. The time difference Δt is quantised in terms of bunch crossings:

$$\Delta n = int(\Delta t/T)$$

[1]If t_0 is measured for both pions, the second in time is chosen, in order to have less contamination from prompt accidental clusters.

where T = 5.43 ns is the bunch crossing period. The measured times are then corrected as follows:

$$t^1_{measured} = t^0_{measured} - \Delta n \cdot T$$

The probability that at least one pion produces a cluster and that this cluster is associated to a track is measured from data and it is $P_\pi = (98.3 \pm 0.1)\%$.

The probability of identifying the correct bunch crossing can be checked with the data using a $K_S \to \pi^+\pi^- \times K_L \to \pi^+\pi^-\pi^0$ sample and comparing the time $t^0_{measured}$ for a photon with the expected time of flight:

$$t_{expected} = L_K/\beta_K c + L_\gamma/c$$

where L_K is the K_L decay length as reconstructed from the drift chamber using the $K_L \to \pi^+\pi^-$ vertex and L_γ is the distance from the K_L vertex and the centroid of the calorimeter cluster (see Fig. 1).

Without imposing any other cut on the K_S pions, the fraction of events is shown in Table 2 as a function of Δn. These results are based on a $K_L \to \pi^+\pi^-\pi^0$ sample corresponding to 21.5 pb^{-1} integrated luminosity.

$\Delta n \leq -2$	$\Delta n = -1$	$\Delta n = 0$	$\Delta n \geq +1$
(1.25 ± 0.06) %	(2.3 ± 0.1) %	(96.2 ± 0.1) %	(0.25 ± 0.03) %

Table 2: Fraction of tagged events as a function of the bunch crossing error.

An error Δn in the bunch crossing determination produces two effects:

1. a wrong t_0 produces a shift in the position of the neutral vertex of $\Delta L_K = -\Delta n \cdot T \cdot \beta c$. For a period of T = 5.43 ns and $\beta \sim 0.2$: $\Delta L_K = -\Delta n \cdot$ 33 cm. This produces a flow of events through the fiducial volume. This effect is the same (at first order) for $K_L \to \gamma\gamma$ and $K_L \to \pi^0\pi^0\pi^0$ and cancels in the ratio.
2. a wrong t_0 changes the number of clusters connected to the neutral vertex and affects the selection efficiency. In this case the effect is different for the two decay channels and does not cancel in the ratio. The selection efficiencies must be evaluated as a function of the bunch crossing error for both channels.

To avoid that the selection efficiencies depend on the bunch crossing error we have to reduce the probability to have a wrong bunch crossing to few per mil. Thus further cuts have been applied to the K_S pions.

Fig. 8 shows the shift in the measured time for the two K_S pions of the $K_S \to \pi^+\pi^- \times K_L \to \pi^+\pi^-\pi^0$ sample with respect to the expected times ($t_{expected} = L/\beta c$), both in the case of correct identification of the bunch crossing (red dots) and in the case of wrong identification of the bunch crossing (black dots).

Applying the cut $|t - L/\beta c| < 2$ ns in the case of just one pion associated ($P_{1\pi} = (30.7 \pm 0.2)\%$) and in the case of both pions associated ($P_{2\pi} = (69.3 \pm 0.1)\%$), reduces the probability to have a wrong bunch crossing identification to 0.6% (see Table 3) with an efficiency of $(96.0 \pm 0.1)\%$ for $K_S \to \pi^+\pi^-$.

Fig. 9 shows the difference of the measured time for a photon from $K_L \to \pi^+\pi^-\pi^0$ decay with respect to the expected time (calculated from the calorimeter cluster position and the

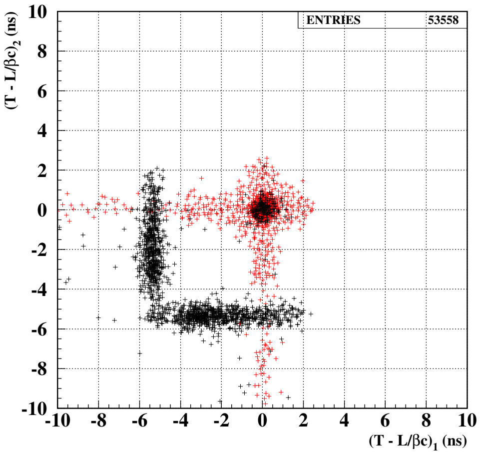

Figure 8: Shift in the measured times of the pions from the K_S decay with respect to the expected times in the case of correct bunch crossing (red dots) and wrong bunch crossing (black dots). A cut of $|t - L/\beta c| < 2$ ns is applied to both pions.

$\Delta n \leq -2$	$\Delta n = -1$	$\Delta n = 0$	$\Delta n \geq +1$
(0.2 ± 0.1) %	(0.3 ± 0.1) %	(99.4 ± 0.1) %	(0.1 ± 0.1) %

Table 3: Fraction of tagged events as a function of the bunch crossing error after the cut $|t - L/\beta c| < 2$ ns applied to the measured times for the K_S pions.

position of the K_L decay vertex reconstructed from the charged tracks) before (black) and after (red) the cut applied to the K_S pions. If the bunch crossing is correctly evaluated all peaks must be centred at zero. The peaks not centred at zero are due to events with a wrongly identified bunch crossing. The final distribution (red histo) shows a residual misidentification of $\sim 0.6\%$.

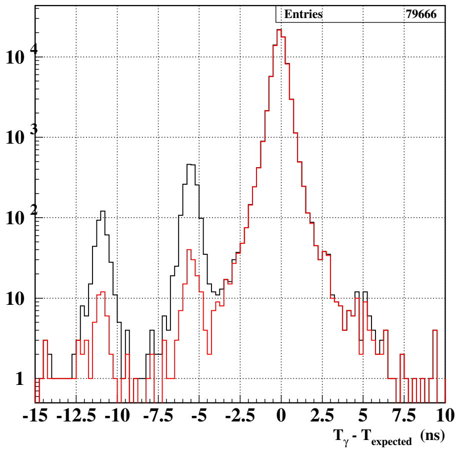

Figure 9: Difference between the measured time for a photon from $K_L \to \pi^+\pi^-\pi^0$ decay and the expected time before (black) and after (red) the cut applied to the K_S pions.

4 Analysis of the $K_L \to \pi^0\pi^0\pi^0$ decay

4.1 The selection

The $K_L \to \pi^0\pi^0\pi^0$ decay has a large branching fraction, 21% and it has practically no competitors between the K_L decays because of the large number of photons. Given the large statistics we downscale the events by a factor $\times 10$. In order to reach a good precision in counting the number of decays, the selection of the $K_L \to \pi^0\pi^0\pi^0$ is as inclusive as possible: we consider all the events with ≥ 3 clusters with the following requirements:
1) energy larger than 20 MeV;
2) distance from any other cluster larger than 40 cm;
3) no association with a charged track.

The main sources of inefficiencies are:
1) the geometrical acceptance;
2) the discriminator threshold;
3) merging with other clusters;
4) accidental association to a charged track;
5) Dalitz decay of one or more π^0.

The only effect of these inefficiencies is to change the relative weight of the populations for events with 3,4,5,6,7,$\geq$ 8 clusters connected with the K_L decay vertex without loosing efficiency on the event selection itself. The Monte Carlo simulation shows that the probability to have at least three neutral clusters connected to a K_L decay vertex in the FV is (99.80 ± 0.01)%.

The total energy of the clusters connected with the neutral vertex is a simple but powerful variable to signal the presence of background. The distribution of the total energy for events with 5,6,7 and $\geq$8 clusters connected to the K_L decay vertex is shown in Fig. 10.

For the categories with 3 and 4 clusters the background is huge (see Fig. 11). A Monte Carlo analysis shows that the main sources of background are:

$K_L \to \pi^+\pi^-\pi^0$ decays where one or two charged pions produce a cluster not associated to a track and both tracks are not associated to the K_L decay vertex.

$K_L \to \pi^0\pi^0$ decays;

machine background that showers in the quadrupoles and generates soft neutral particles.

To reduce the contamination from machine background producing low energy clusters close to the beam pipe, for 3-cluster events we require at least two clusters on the barrel and among them at least one cluster with $E > 50$ MeV; for 4-cluster events we require at least one cluster on barrel with $E > 50$ MeV. The probability that a photon from a $K_L \to \pi^0\pi^0\pi^0$ event produces a cluster with $E > 50$ MeV has been evaluated from data using the 6-cluster sample and is $\epsilon_{E>50\,MeV} = (81.9 \pm 0.1)$ % (Fig. 18). This number must be weighted with the probabilities a given number of clusters on the barrel in order to get the efficiency of the cuts. Since the number of clusters on barrel depend only from the geometry we rely on Monte Carlo to evaluate this number. The distributions of the number of clusters on barrel for the 3- and 4- clusters populations are shown in Fig. 12.

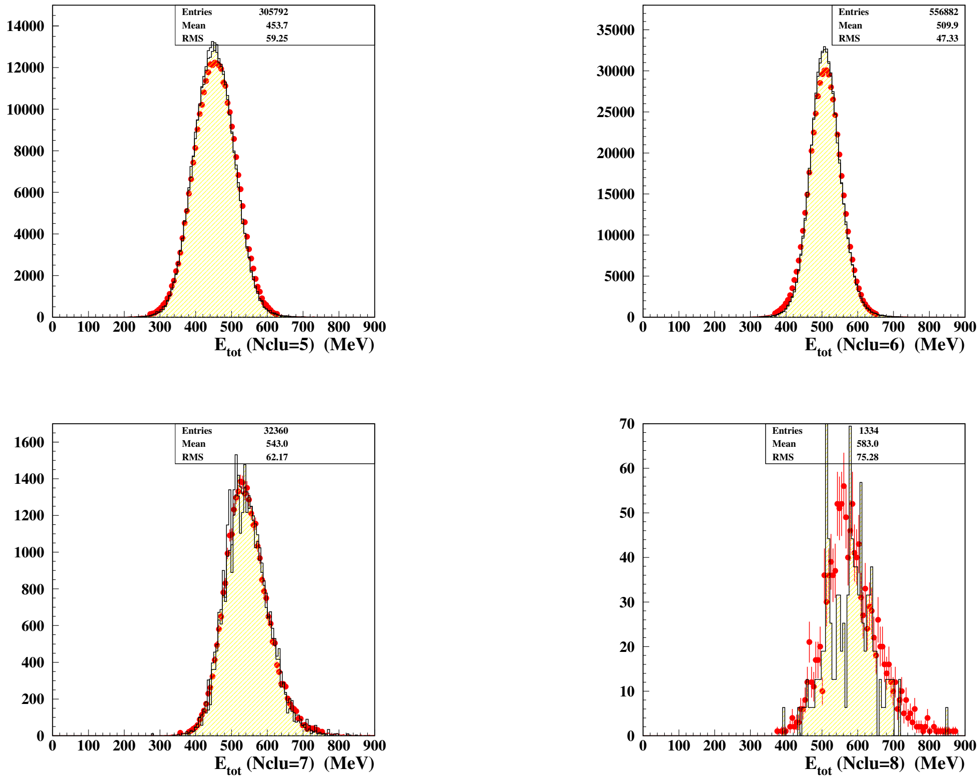

Figure 10: Total energy distributions for events with with 5,6,7 and ≥8 clusters connected to the K_L decay vertex. The solid line is Monte Carlo for $K_L \rightarrow$all events, yellow histo is Monte Carlo for $K_L \rightarrow \pi^0\pi^0\pi^0$ events, the dots are data.

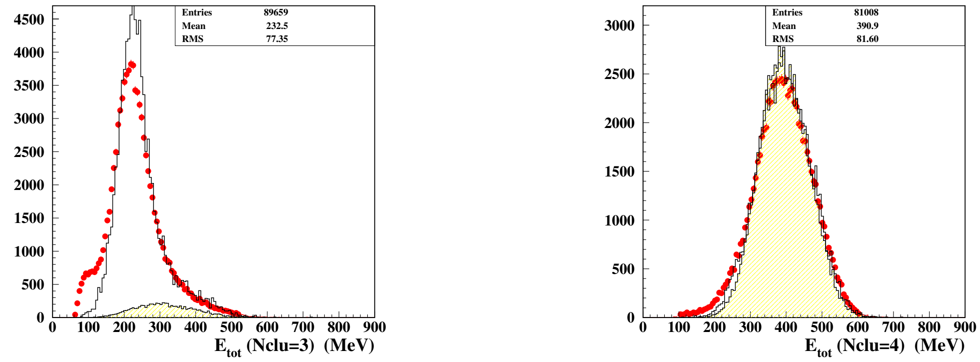

Figure 11: Total energy distributions for events with 3 and 4 neutral clusters connected to theK_L decay vertex. The solid line is Monte Carlo for $K_L \rightarrow$all events, yellow histo is Monte Carlo for $K_L \rightarrow \pi^0\pi^0\pi^0$ events, the dots are data.

The efficiency of these two cuts, are respectively, $\epsilon_{\,sel,N=3} = (81.9 \pm 0.1)\%$ and $\epsilon_{\,sel,N=4} = (98.3 \pm 0.1)\%$.

An event with only 3 clusters connected with the K_L decay vertex is accepted only if an additional cluster is found in QCAL within a time window of 10 ns with respect to the K_L decay time (Fig. 13). The efficiency evaluated with Monte Carlo is $\epsilon_{qcal} = (52 \pm 2)\%$.

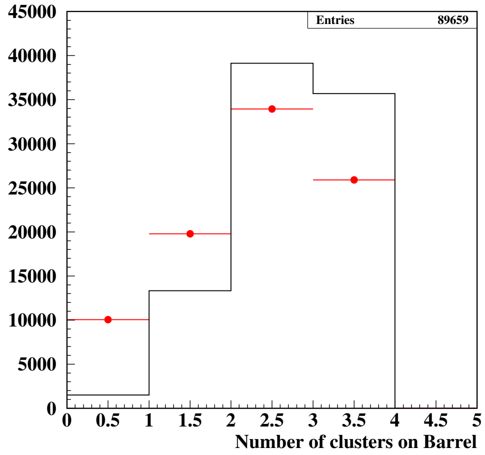

Figure 12: Distributions of the number of clusters on barrel for 3-cluster events (left) and 4-cluster events (right). Red dots are data, solid histo is Monte Carlo. Data are before any selection cut.

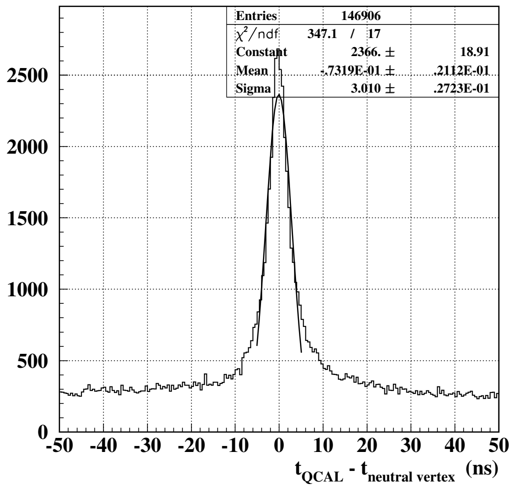

Figure 13: Time distribution of clusters in QCAL with respect to the K_L decay time for events with 3 clusters connected to the K_L vertex (data). A 3-cluster event is accepted only if an additional cluster in QCAL is found within a time window of $3\sigma_t = 10$ ns.

The $K_L \to \pi^+\pi^-\pi^0$ background is rejected imposing a veto (*track veto*) on the events with charged tracks not belonging to the K_S *decay chain* [2] and with the first hit at a distance of less than 30 cm from the position of the K_L decay vertex (see Fig. 14).

The track veto has an efficiency of 40% for events with $K_L \to$2 tracks + n γ and therefore rejects about 60% of the $K_L \to \pi^0\pi^0\pi^0$ events with Dalitz decays.

The track veto is applied only to the 3- and 4- cluster populations but it has been studied for all the populations of neutral clusters connected to the K_L decay vertex.

[2]The K_S *decay chain* is defined as the set of tracks connected, directly or through a chain of vertices and tracks, to the $K_S \to \pi^+\pi^-$ vertex.

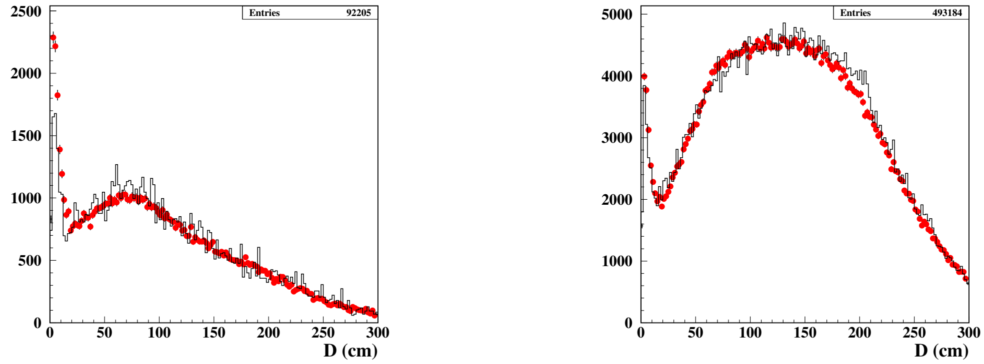

Figure 14: Distribution of the distance between the K_L decay vertex and the first hit in the drift chamber of charged tracks not associated to the K_S decay chain for < 5 (left) and ≥ 5 (right) neutral clusters associated to the K_L vertex. Red dots are data, solid line is Monte Carlo for $K_L \to$all. The peak at zero is due both to $K_L \to \pi^+\pi^-\pi^0$ and Dalitz decays for the < 5 cluster population and only to Dalitz decays for the ≥ 5 cluster population.

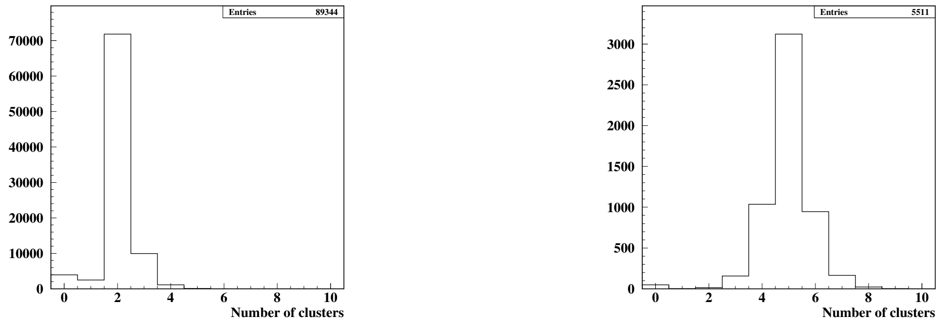

Figure 15: Monte Carlo distribution of the number of neutral clusters connected to the K_L decay vertex for $K_L \to \pi^+\pi^-\pi^0$ events (left) and for $K_L \to \pi^0\pi^0\pi^0$ with Dalitz decays (right).

In Fig. 16 the data are compared with a Monte Carlo simulation of events $K_S \to \pi^+\pi^- \times K_L \to$all. The 5-cluster population, which is background free, is used to estimate the efficiency of the track veto on $K_L \to \pi^0\pi^0\pi^0$ events with Dalitz decays. The probability to have a Dalitz decay in a $K_L \to \pi^0\pi^0\pi^0$ event is $p = 3 \times BR_{\mathrm{Dalitz}} = 3.6\%$ [1]. From Monte Carlo (Fig. 15, right) 56 % of $K_L \to \pi^0\pi^0\pi^0$ with Dalitz decays has 5 neutral clusters. Since the 5-cluster population accounts for $\sim$ 31.5% of the total (see Table 4), the relative amount of Dalitz decays on the 5-cluster population is $\sim$ 6.4%. The drop of efficiency of 4% observed both in data and Monte Carlo for the 5-cluster population (see Fig. 16) is therefore consistent with $\epsilon_{TV} \sim 40\%$.

For the 4-cluster events the drop in the efficiency observed in data is reproduced at % level by the Monte Carlo and is compatible with the amount of Dalitz decays and $K_L \to \pi^+\pi^-\pi^0$ events (Fig. 15) foreseen by Monte Carlo for this population. A difference of 20% between data and Monte Carlo is instead observed in the 3-cluster population: this is due to a bad estimate of the contamination of events with charged tracks. Since the 3-cluster population accounts for 0.4 % of the total (Table 4), a 20% difference has a 0.1% effect on the total counting. This small effect has been anyhow taken into account in the evaluation of systematics. The final distribution for the 3- and 4-cluster events is shown in Fig. 17.

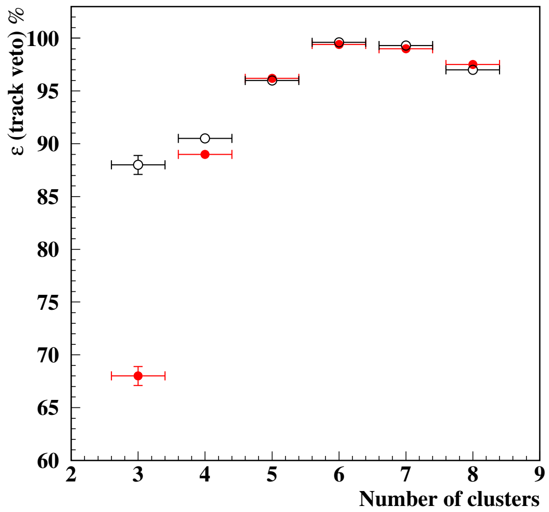

Figure 16: Efficiency of the track veto for $K_L \rightarrow \pi^0\pi^0\pi^0$ as a function of the number of neutral clusters connected to the K_L decay vertex. Red dots are data, open circles Monte Carlo for $K_L \rightarrow$all.

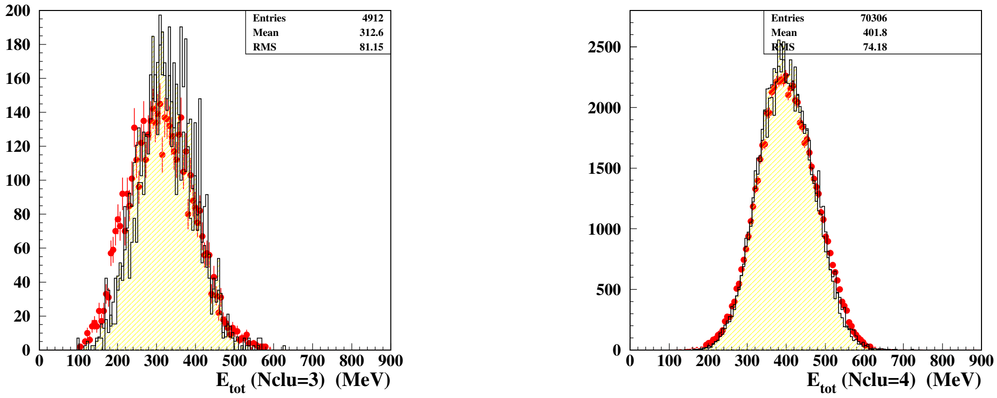

Figure 17: Final distributions of the total energy for the events with 3 and 4 clusters. Dots are data, solid line is Monte Carlo.

Fig. 18 shows the inclusive distribution of the cluster energy for selected $K_L \rightarrow \pi^0\pi^0\pi^0$ events. Fig. 19 shows the distribution of the number of clusters connected to the K_L decay vertex. The probabilities of the different populations are shown in Table 4. The difference between data and Monte Carlo for the events with ≥ 5 clusters is due to splitted clusters. The probability P_S that a single incident photon produces two clusters is estimated from data using the relation:

$$P_S = \frac{p_7}{6 \cdot p_6} = 1\% \quad \text{(MC value: 0.5\%)}.$$

where p_7 and p_6 are the probabilities to have a 6- or 7- cluster event on the $K_L \rightarrow \pi^0\pi^0\pi^0$ sample (see Table 4).

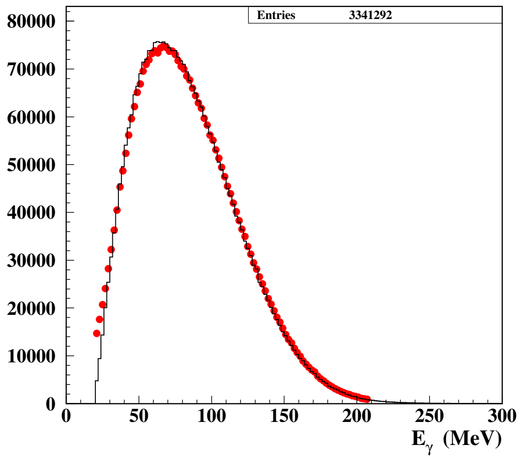

Figure 18: Distribution of the energy of single cluster for selected $K_L \to \pi^0\pi^0\pi^0$ events. Dots are data, the solid line is Monte Carlo.

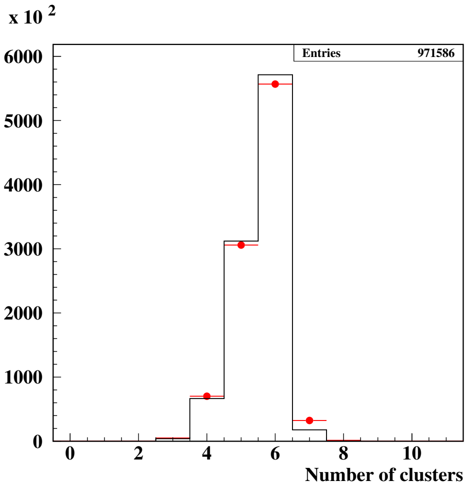

Figure 19: Distribution of clusters connected to the K_L decay vertex. Dots are data, the solid histo is Monte Carlo. Data and Monte Carlo are normalized to the same number of events.

Number of clusters	Data	Monte Carlo
3	0.37 ± 0.02 %	0.35 ± 0.04 %
4	7.2 ± 0.1 %	7.3 ± 0.1 %
5	31.5 ± 0.1 %	32.2 ± 0.2 %
6	57.4 ± 0.1 %	58.4 ± 0.2 %
7	3.3 ± 0.1 %	1.7 ± 0.1 %
≥ 8	0.1 %	0.03 %

Table 4: Fraction of events with ≥ 3 neutral clusters connected to the K_L decay vertex.

4.2 Accidental clusters contamination

The contamination of accidental clusters originated by machine background depends on the rate of machine background events and on the width of the time window (TW) chosen to build a K_L decay vertex from photons (see Fig. 3, left). The rate of clusters due to machine background depends on the run conditions and is measured run by run using cosmic rays [5]. We assume a conservative value of 2.8 $\cdot 10^{-3}$/ns for accidental clusters with energy above 20 MeV. The width of the time window is $6{\cdot}\sigma_t$ where $\sigma_t = \sigma(L_K)/(\beta_K \gamma_K c)$ and $\sigma(L_K)$ shown in Fig. 1. Given an average K_L path length of $\sim$ 100 cm, TW turn out to be $\sim$ 1.8 ns. The probability that a single accidental cluster above 20 MeV enters in the time window is therefore $P_A(1) \sim 0.5 \cdot 10^{-3}$, the probability to have two accidentals in the same time window being negligible. The number $N^{obs}_{\geq 3}$ of observed events with more than 3 cluster is related to the distribution $\{n_i\}$ in absence of accidentals as follows:

$$N^{obs}_{\geq 3} = n_2 \cdot P_A(1) + n_{\geq 3}$$

The fractional variation in the event counting due to the presence of accidentals is therefore negligible:

$$\frac{N^{obs}_{\geq 3} - n_{\geq 3}}{n_{\geq 3}} = \frac{n_2 \cdot P_A(1)}{n_{\geq 3}} \simeq 2 \cdot 10^{-3} \times 0.5 \cdot 10^{-3} \simeq 10^{-6}$$

4.3 Background evaluation

According to Monte Carlo simulation a residual background affects the populations with 3, 4 and 5 neutral clusters and is mainly due to $K_L \to \pi^0\pi^0$ and $K_L \to \pi^+\pi^-\pi^0$ decays. The final composition of these populations after the selection cuts from Monte Carlo is shown in Table 5.

N	background channel	fraction	background channel	fraction
3	$K_L \to \pi^+\pi^-\pi^0$	$(9.6 \pm 0.3)\%$	$K_L \to \pi^0\pi^0$	$(9 \pm 1)\%$
4	$K_L \to \pi^+\pi^-\pi^0$	$(2.7 \pm 0.1)\%$	$K_L \to \pi^0\pi^0$	$(4.3 \pm 0.2)\%$
5	$K_L \to \pi^+\pi^-\pi^0$	-	$K_L \to \pi^0\pi^0$	$\sim 10^{-4}$

Table 5: Percentages of background events in the 3-, 4- and 5- cluster populations after the selection (Monte Carlo).

4.4 FILFO and trigger effect

With a sample of $5.6 \cdot 10^6$ triggers, collected in three different runs, we reconstruct the events with and without the application of the FILFO filter. Table 6 shows the result. The action of the filter on $K_L \to \pi^0\pi^0\pi^0$ events is negligible: over 2165 selected events the result is exactly the same with or without the filter.

The trigger efficiency for $K_S \to \pi^+\pi^- \times K_L \to \pi^0\pi^0\pi^0$ events is measured in two different ways. Since the two methods are independent, we evaluate the efficiency using both results. A detailed discussion on the methods is given in reference [6].

The first method is entirely based on the data and, together with the total efficiency, gives also the partial efficiencies for the $K_S \to \pi^+\pi^-$ and the $K_L \to \pi^0\pi^0\pi^0$ part of the event.

Run	Triggers	Preselection		Final selection (FV)	
		No filfo	filfo	no filfo	filfo
22001	2000000	1826	1818	779	779
22406	1600000	1455	1454	630	630
23002	2000000	1809	1802	756	756
	5600000	5090	5074	2165	2165

Table 6: Summary of the FILFO action on $K_L \rightarrow \pi^0\pi^0\pi^0$ events. We compare the numbers of events obtained after the preselection and in the final selection with and without the filter.

In the second method the Monte Carlo is used to evaluate the correlation between the DC and the EMC trigger. The correlation factor is very small: $(-6.2 \pm 1.2) \times 10^{-4}$. The results obtained with the two methods are in good agreement (see Table 7).

	$\epsilon_1(\%)$	$\epsilon_2(\%)$
$K_L \rightarrow \pi^0\pi^0\pi^0$	98.70 ± 0.24	
$K_S \rightarrow \pi^+\pi^-$	50.6 ± 2.5	
Total	99.88 ± 0.04	99.90 ± 0.03

Table 7: Trigger efficiency evaluated with the two methods; for the first method the partial efficiencies are also quoted. The error is the systematic one.

The effect of the cosmic veto on the $K_L \rightarrow \pi^0\pi^0\pi^0$ events has been studied. We found 537 events with the cosmic veto fired, corresponding to 0.055 % of the total statistic, 96 in the 2001 and 441 in the 2002 data sample. All the 441 events of the 2002 data sample have been recognised by the level 3 filter as events with 2 tracks from the origin and then they are not been down-scaled by the trigger. The 96 events of the 2001 data sample, instead, must be multiplied by the downscaling factor of 5. This is, anyhow, a correction of 0.05 % and therefore fully negligible.

4.5 Event counting

The number of events is:

$$N_{\pi^0\pi^0\pi^0} = \frac{N_3 + N_4 + N_5 + N_6 + N_7 + N_{\geq 8} + N_{\mathrm{Dalitz}}}{\epsilon_{\,downscale} \cdot \epsilon_{\,trg} \cdot \epsilon_{\,nv}}$$

where N_i, $i = 3, 4, 5, 6, 7, 8$, is the number of events with i neutral clusters connected to the K_L decay vertex, $\epsilon_{\,downscale} = 10\%$ is the downscaling factor, $\epsilon_{\,trg} = (99.9 \pm 0.03)\%$ is the trigger efficiency and $\epsilon_{\,nv} = (99.8 \pm 0.01)\%$ is the probability to have at least three neutral clusters connected to a K_L decay vertex in the FV. N_3 and N_4 are obtained after background subtraction and correction for the selection efficiencies:

$$N_3 = \frac{(N_3(\mathrm{obs}) - \mathrm{bkg}_{N=3})}{\epsilon_{\,sel,N=3} \cdot \epsilon_{\,qcal}}$$

$$N_4 = \frac{(N_4(\mathrm{obs}) - \mathrm{bkg}_{N=4})}{\epsilon_{\,sel,N=4}}$$

where $\epsilon_{sel,N=3} = (81.9\pm0.1)\%$, $\epsilon_{qcal} = (52\pm2)\%$, $\epsilon_{sel,N=4} = (98.3\pm0.1)\%$ and the estimated background is given in table 5. We assume to know the background in the $N = 3$ and $N = 4$ populations at 20 % level. For the 3-cluster population we assume a systematic error of 10% on the estimate of ϵ_{qcal}. We obtain:

$$N_3 = 9927(1 \pm 4\%(\mathrm{bkg}) \pm 10\%(\epsilon_{qcal})) = 9927 \pm 1069_{syst}$$

$$N_4 = 66515(1 \pm 1.4\%(\mathrm{bkg}) = 66515 \pm 931_{syst}$$

N_{Dalitz} is obtained assuming that $p = 21.5\%$ of the Dalitz decays in $K_L \to \pi^0\pi^0\pi^0$ events are included in the N_3 and N_4 populations and that 60% is rejected by the track veto. We assume a 10% systematic error due to the knowledge of p and 10 % systematic error due to the estimate of the efficiency of the track veto:

$$N_{Dalitz} = 3 \cdot BR(\pi^0 \to e^+e^-\gamma) \times p \times (1 - \epsilon_{TV}) = 4472(1 \pm 3.6\%(BR) \pm 10\%(p) \pm 10\%(\epsilon_{TV})) = 4472 \pm 632_{syst}$$

The final number of events is

$$N_{\pi^0\pi^0\pi^0} = 9802207 \; (1 \pm 0.0010_{\mathrm{stat}} \pm 0.0016_{\mathrm{syst}})$$

To check the stability of the result we plot in Fig. 20 the number of $K_L \to \pi^0\pi^0\pi^0$ events per nb^{-1} before background subtraction and correction for the efficiencies. Each point has been calculated for a luminosity of 3 pb^{-1}.

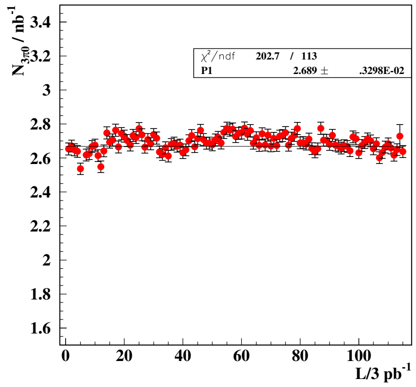

Figure 20: Counting stability. Each point is calculated for a luminosity of 3 pb^{-1}.

To check the uniformity of the $K_L \to \pi^0\pi^0\pi^0$ vertex reconstruction in the FV we have measured the proper time decay distribution. The fit of the distribution, Fig. 21, gives $\tau = (51.6 \pm 0.4)$ ns, in good agreement with the world average, $\tau = (51.7 \pm 0.4)$ ns [1].

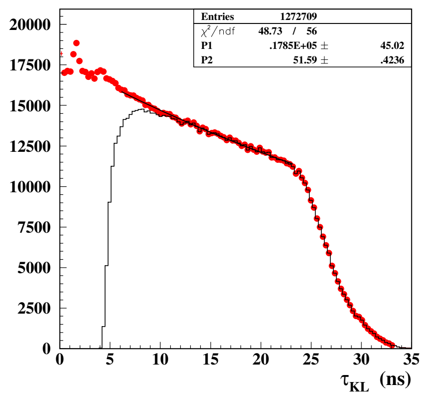

Figure 21: Proper time decay distribution of K_L , from K_L to $\pi^0\pi^0\pi^0$ events. Red dots are data selected by removing the inner boundary of FV, solid histo are data collected in the chosen FV. The fit has been performed with the function $f(t) = p_1 e^{-t/p_2}$ in the region of FV 40 cm $< r <$ 155 cm.

5 Analysis of the $K_L \to \gamma\gamma$ decay

The $K_L \to \gamma\gamma$ decay is a very clean signal. The contamination from other processes is so small that the most dangerous background, together with the $K_L \to \pi^0\pi^0\pi^0$ decay, is the CP-violating decay $K_L \to \pi^0\pi^0$. A very high rejection power against background and a high efficiency can be reached with simple kinematical cuts.

5.1 The preselection

Very loose cuts are applied at first level to make a preselection of the event sample. To pass the preselection an event must have at least two calorimeter clusters not associated to tracks with the following properties:

1. energy of each cluster $E_\gamma > 100$ MeV;
2. relative angle between the photon momenta projected in the plane transverse to the K_L momentum $\psi > 150°$;
3. total energy $E = E_{\gamma 1} + E_{\gamma 2} > 350$ MeV;
4. time difference of the two most energetic clusters smaller than 15 ns;
5. the decay length of the two most energetic clusters must satisfy the relation:

$$\Delta l_K = |l_{k1} - l_{k2}| < 4 \cdot \sigma_{\gamma\gamma}(l_K)$$

$\sigma_{\gamma\gamma}(l_K) = 1.73 + 0.0033 \cdot l_K$ cm is evaluated from the data (see Fig. 22).

The geometrical acceptance and the preselection efficiency are evaluated with Monte Carlo. The efficiency for a photon to produce a cluster with energy larger than 100 MeV is $\epsilon_\gamma = (99.6 \pm 0.1)\%$. The efficiency to produce two clusters with energy larger than 100 MeV is $\epsilon_{\gamma\gamma} = (92.6 \pm 0.1)\%$. The values of the efficiency of the preselection cuts are shown in Table 8. The systematic error of Δl_k and ψ efficiencies is evaluated moving the cuts around the

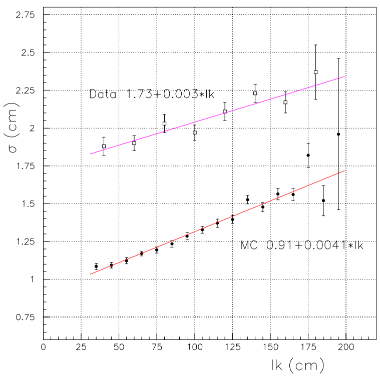

Figure 22: $\sigma(l_{k1} - l_{k2})$ as a function of $l_k = (l_{k1} + l_{k2})/2$ for $K_L \to \gamma\gamma$ data and Monte Carlo events. The result of a fit with a straight line is shown.

chosen value and fitting the signal content in the invariant mass distribution, Fig. 26 upper right, for a given cut. In order to remove the statistical fluctuation of the signal distribution, we plot the difference $\Delta N = N_{i+1} - N_i$ of signal content versus the difference $\Delta\epsilon = \epsilon_{i+1} - \epsilon_i$ of the cut efficiencies assuming the first point $(N, \epsilon) = (0{,}0)$. The errors on the points are the statistical ones.

The maximum displacement between the measured values and the straight line that gives the best fit is an estimate of the systematic error in the evaluation of efficiency (Fig. 23).

cut	ϵ (cut) (%)
$2\times(E > 100$ MeV)	$(92.6 \pm 0.1_{stat})$ %
$E > 350$ MeV	$(99.88 \pm 0.02_{stat})$ %
$\Delta l_k < 4 \cdot \sigma$	$(98.5 \pm 0.1_{stat} \pm 0.2_{syst})$ %
$\Delta t < 15$ ns	$(99.89 \pm 0.02_{stat})$ %
$\psi > 150°$	$(98.4 \pm 0.1_{stat} \pm 0.4_{syst})$ %
total	$(89.5 \pm 0.2_{stat} \pm 0.4_{syst})$ %

Table 8: Efficiency of the preselection cuts.

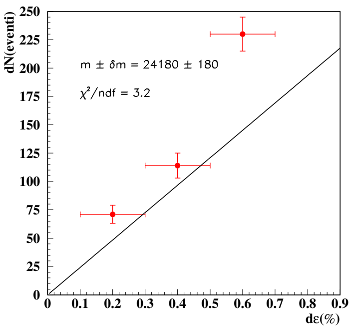

Figure 23: ΔN vs $\Delta\epsilon$ (see text) for different cuts in ψ in the range $140° < \psi < 165°$. The errors on the points are the statistical ones. The maximum displacement between the measured points and the straight line that gives the best fit is $\delta = 0.4\%$.

5.2 The selection

The signal is selected with two cuts that exploit the two body $K_L \to \gamma\gamma$ decay kinematics. The first cut is done on the energy of the K_L in the laboratory, E^*, obtained making a Lorentz transformation from the center of mass where the energy of the photons is equal to $M_K/2$:

$$E^* = E^*_{\gamma 1} + E^*_{\gamma 2}$$

with

$$E^*_{\gamma j} = \frac{M_K/2}{\gamma_K(1 - \beta_K\ \hat{p}_{\gamma j} \cdot \hat{p}_K)}$$

E^* depends on:

- the direction ($\hat{p}_K$) and the module (β_K, γ_K) of the momentum of the K_L, both related to the measurement of the K_S momentum ($\vec{p}_{K_L} = \vec{p}_\phi - \vec{p}_{K_S}$);
- the directions of the photons ($\hat{p}_{\gamma j}$) measured by the position of the neutral vertex and of the calorimeter cluster centroid.

Fig. 24 shows the distribution of E^*_{tot} after the preselection. Monte Carlo signal and background samples are normalized to the expected S/B ratio after the preselection assuming a $BR(K_L \to \gamma\gamma) = 5.9 \cdot 10^{-4}$ [1]. A clear peak around 510 MeV is already visible before any selection. In the analysis we require

$$|E^* - \mu^*| < 5 \cdot \sigma^*$$

where $\sigma^* = 1.8$ MeV and $\mu^* = 510.0$ MeV are evaluated from a fit to the E^* distribution.

The second cut is done on the angle α between the K_L momentum reconstructed from the two photons momenta

$$\vec{p}^*_{\gamma\gamma} = E^*_{\gamma 1}\ \hat{p}_{\gamma 1} + E^*_{\gamma 2}\ \hat{p}_{\gamma 2}$$

and the K_L momentum reconstructed from the K_S and the ϕ ($\vec{p}_{K_L} = \vec{p}_\phi - \vec{p}_{K_S}$)

$$\cos\alpha = \frac{\vec{p}^*_{\gamma\gamma} \cdot \vec{p}_{K_L}}{|\vec{p}^*_{\gamma\gamma}||\vec{p}_{K_L}|}$$

In Fig. 25 the distribution of α is shown before and after the cut on E^*. In the analysis we require $\alpha < 15°$.

The angle α depends on:

- the direction ($\hat{p}_K$) and the module (β_K, γ_K) of the momentum of the K_L, both related to the measurement of the K_S momentum ($\vec{p}_{K_L} = \vec{p}_\phi - \vec{p}_{K_S}$);
- the angle between the two photons evaluated using the position of the neutral vertex and the positions of the calorimeter cluster centroid.

The invariant mass of the two photons $M_{\gamma\gamma}$ is used as a control variable. Fig. 26 shows how the $M_{\gamma\gamma}$ distribution changes as a function of the applied cuts. Data are fitted with a linear combination of the Monte Carlo distributions for data and background. The result of the fit gives the number of events for the two populations.

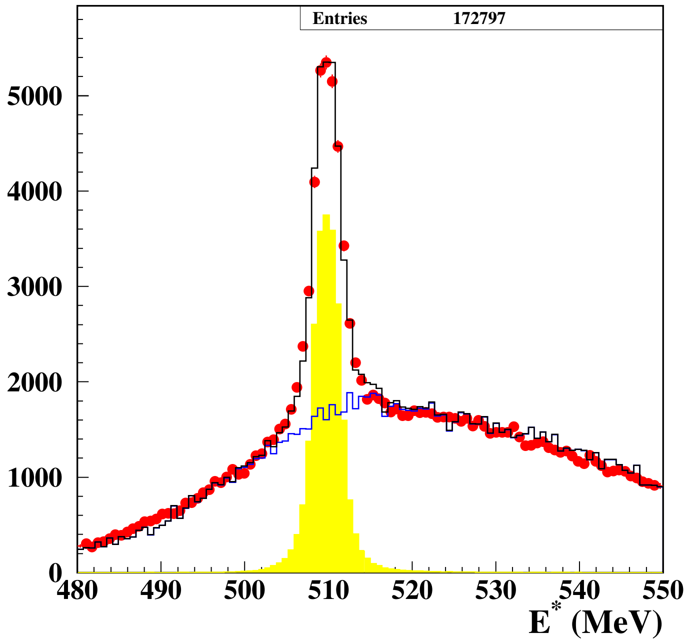

Figure 24: E^* distributions for data (red dots), Monte Carlo signal (yellow histo), Monte Carlo background (blue histo) and Monte Carlo signal+background (black histo).

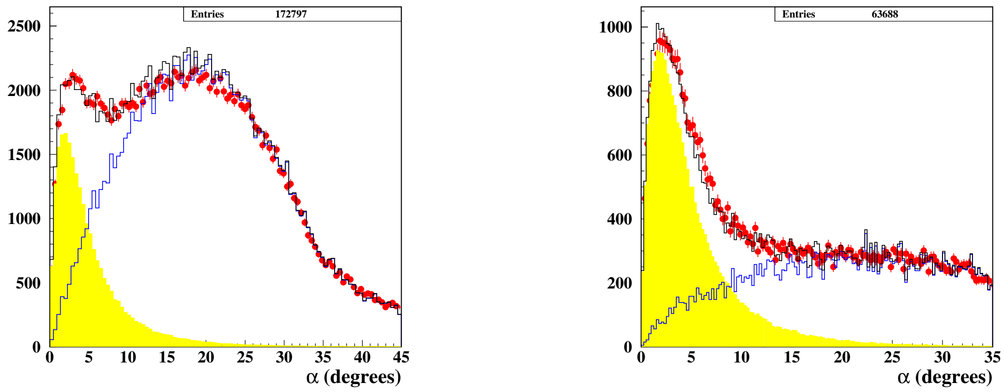

Figure 25: Distribution of α before (left) and after (right) the E^* cut. Red dots are for data, yellow histo is Monte Carlo signal, blue histo is Monte Carlo background and black histo Monte Carlo signal+background.

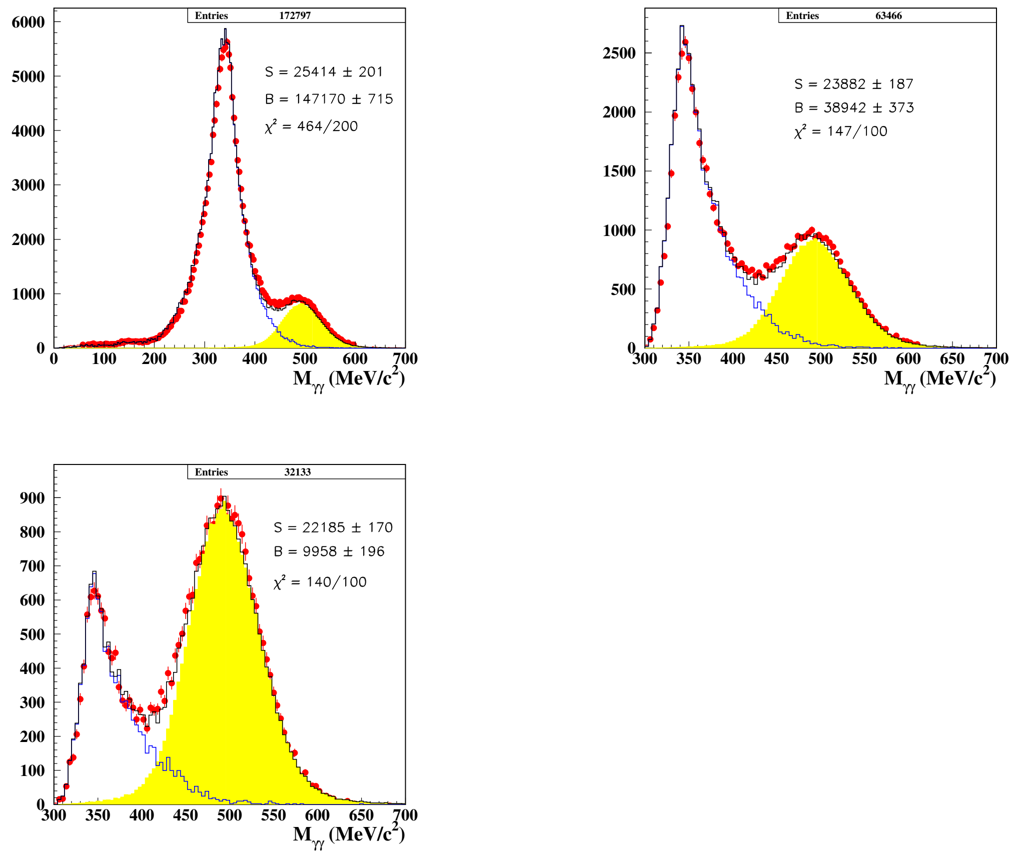

Figure 26: Invariant mass distribution for different cuts: after the preselection (upper left), after the E^* cut (upper right) and after the α cut (bottom right).

5.3 Selection efficiency

The efficiency of the selection cuts are evaluated from the data using a subsample of the signal itself. A Monte Carlo analysis shows that a clean subsample of the signal can be obtained using the following cuts:

1. total energy measured by the calorimeter greater than 510 MeV (see Fig. 27 right);
2. events with more than two neutral clusters are vetoed if there is at least a third cluster in a time window of $\Delta t = |T - L_\gamma/c - L_{K_L}/(\beta c)| < 3 \cdot \sigma_t = 1$ ns; σ_t is defined by the two most energetic clusters (see Fig. 27 left);
3. $|E^* - \mu^*| < 5\sigma^*$ to study the effect of the cut on the distribution of α;
4. $\alpha < 10°$ to study the effect of the cut on the distribution of E^*.

The Monte Carlo simulation shows, in addition, that the correlation between variables is negligible in all cases but for the couple of variables $E^* - \alpha$ since both depend on the measurement of the K_L direction. The correlation has been computed with Monte Carlo and taken into account in the evaluation of the efficiency. The systematic error of the E^* and α efficiencies is evaluated moving the cuts around the chosen value and fitting the signal content in the invariant mass distribution for a given cut. In order to remove the statistical fluctuation of the signal distribution, we plot the difference $\Delta N = N_{i+1} - N_i$ of signal content versus the difference $\Delta\epsilon = \epsilon_{i+1} - \epsilon_i$ of the cut efficiencies assuming the first point (N, ϵ) = (0,0). The errors on the points are the statistical ones. The maximum displacement between the measured values and the straight line that gives the best fit is an estimate of the systematic error in the evaluation of efficiency.

The maximum displacement is 0.2% and 0.3% for the E^* and the α cut respectively (Fig. 28).

The systematic error due to the background subtraction has been estimated changing the background content in the fit up to ±16%. The effect on the signal is 10 times smaller (Fig. 29). The accuracy in the knowledge of the background shape of the Monte Carlo distribution has been estimated by using the difference between the two cumulative functions of the invariant mass distribution for data and Monte Carlo for a sample of background events. This sample has been selected by performing anti-cuts on the same variables, E^* and α, used for the selection of the signal. The maximum difference in this difference is ±3% (Fig. 30) and turns out in a systematic error of 0.3% (Fig. 29).

The efficiencies for the various analysis cuts are summarised in Table 9.

cut	ϵ
ϵ (preselection)	$(89.5 \pm 0.2_{stat} \pm 0.4_{syst})$ %
$\lvert E^* - \mu^*\rvert < 5 \cdot \sigma$	$(98.5 \pm 0.2_{stat} \pm 0.2_{syst})$ %
$\alpha < 15°$	$(92.5 \pm 0.3_{stat} \pm 0.3_{syst})$ %
ϵ (tot)	$(81.5 \pm 0.4_{stat} \pm 0.5_{syst})$ %

Table 9: Efficiencies of the selection cuts.

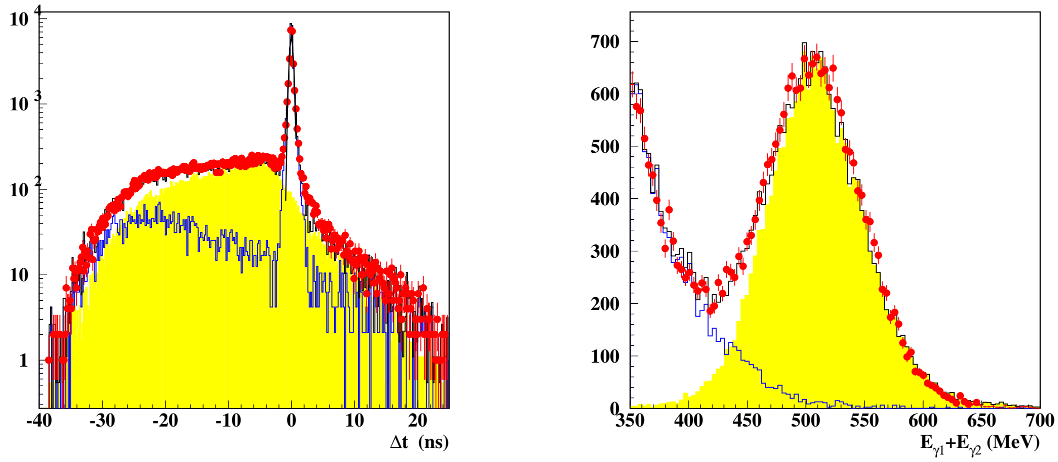

Figure 27: Δt (left) and total energy (right) distributions for data (red dots), Monte Carlo signal (dashed histo), Monte Carlo background (blue histo) and Monte Carlo signal+background (black histo).

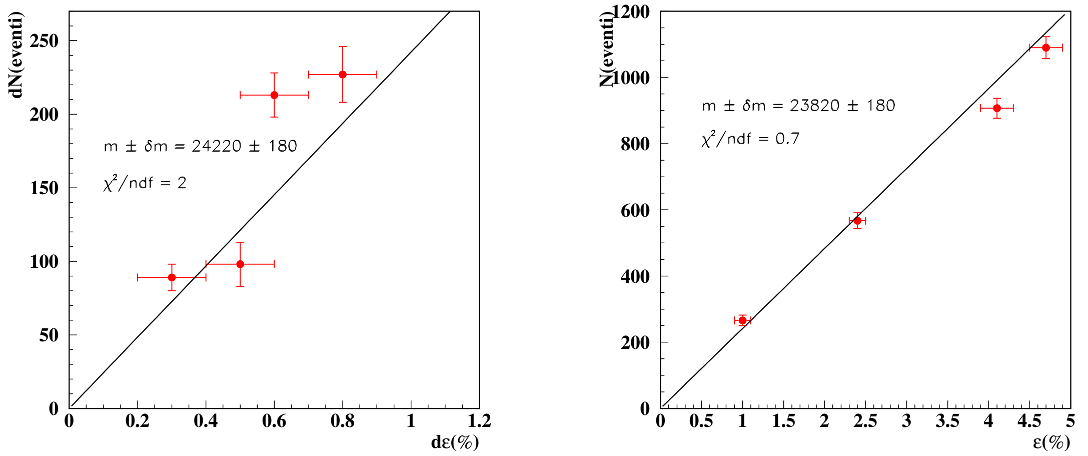

Figure 28: ΔN vs $\Delta\epsilon$ (see text) for different cuts: $|E^* - \mu^*| < n \cdot \sigma$ for $3 \leq$ n ≤ 6 (left) and $\alpha < \alpha^*$ for $10° \leq \alpha^* \leq 22°$ (right). The errors on the points are the statistical ones. The maximum displacement is 0.2% for E^* and 0.3% for α.

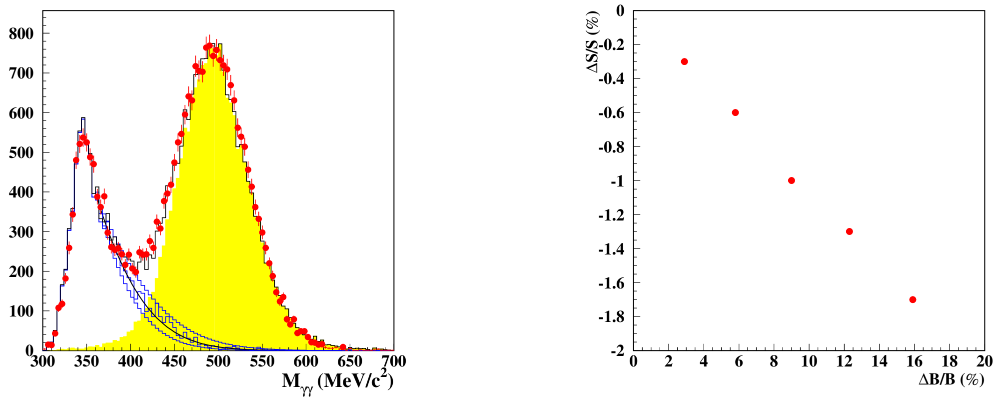

Figure 29: The background content in the signal region has been changed by an amount of $\pm 16\%$ by parametrizing its tail and moving the values of the parameters (right). The effect on the signal fit is 10 times smaller (left).

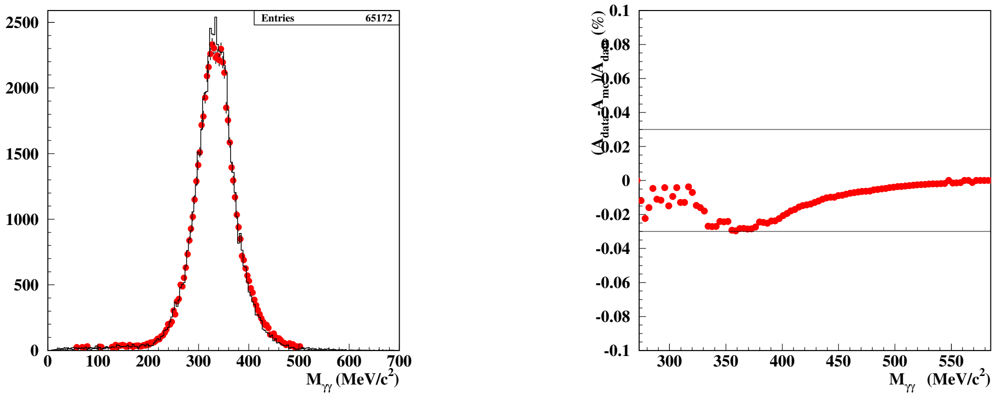

Figure 30: The accuracy in the knowledge of the background shape of the Monte Carlo distribution has been estimated by using the difference between the two cumulative functions (right) of the invariant mass distribution for data and Monte Carlo for a pure sample of background events (left).

5.4 FILFO and trigger effect

The effect of the FILFO filter on the selection of $K_L \to \gamma\gamma$ events has been studied with Monte Carlo. We run the reconstruction program on the same sample of simulated $\gamma\gamma$ events with and without the application of the filter. At the end of the analysis (including FILFO) we count 46778 events while without applying the filter the events are 46813. The fractional variation in the number of events is 0.07 %.

The trigger efficiency of $K_L \to \gamma\gamma$ events is evaluated in the same way as for $K_L \to \pi^0\pi^0\pi^0$ decays. The correlation factor between the DC trigger and the EMC trigger obtained with Monte Carlo is -0.0022 ± 0.0005. Table 10 shows the result of the $K_L \to \gamma\gamma$ trigger analysis.

The effect of the cosmic veto on the $K_L \to \gamma\gamma$ events has been studied. We found 28 events with the cosmic veto fired, corresponding to 0.1 % of the total statistic, 7 in the 2001 and 21 in the 2002 data sample. All the 21 events of the 2002 data sample have been recognised by

Trigger	$\epsilon_1(\%)$	$\epsilon_2(\%)$
$K_L \to \gamma\gamma$	95.5 ± 1.5	
$K_S \to \pi^+\pi^-$	51.1 ± 1.3	
Total	99.62 ± 0.14	99.57 ± 0.04

Table 10: Trigger efficiency for $K_L \to \gamma\gamma$ evaluated with the same methods as for $K_L \to \pi^0\pi^0\pi^0$; for the first method the partial efficiencies are also quoted. The error is the systematic one.

the level 3 filter as events with 2 tracks from the origin and then no downscaling factor has been applied to them by the trigger. The 7 events of the 2001 data sample, instead, must be multiplied by the downscaling factor of 5. We have taken it into account by including this effect in the trigger efficiency.

5.5 Event counting

The number of $K_L \to \gamma\gamma$ events evaluated from the fit to the $M_{\gamma\gamma}$ distribution is $N_{\gamma\gamma}(fit) = 22185 \pm 170 = 22213 \pm 170$. The selection efficiency, including all contributions, is $\epsilon_{tot} \cdot \epsilon_{trg} = 0.8104 \pm 0.0033_{stat} \pm 0.0053_{syst} = 0.8104 \pm 0.0062$. The systematic error on the number of events is $\pm 0.83\%$, 0.77 % from efficiencies evaluation and 0.3 % from background subtraction. The number of events is

$$N_{\gamma\gamma} = 27375\,(1 \pm 0.0077_{stat} \pm 0.0083_{syst})$$

6 The ratio R $= \Gamma(K_L \to \gamma\gamma)/\Gamma(K_L \to \pi^0\pi^0\pi^0)$

For the ratio we obtain:

$$R = \frac{N_{\gamma\gamma}}{N_{\pi^0\pi^0\pi^0}} = \frac{27375\ (1 \pm 0.0077_{stat} \pm 0.0083_{syst})}{9802207\ (1 \pm 0.0010_{stat} \pm 0.0016_{syst})}$$

$$R = (2.793 \pm 0.022_{stat} \pm 0.024_{syst}) \times 10^{-3}$$

To show the stability of the result we divide the data sample in eleven subsamples of 30 pb^{-1} each. The result is shown in Fig. 31.

7 Conclusions

A measurement of the ratio $R = \Gamma(K_L \to \gamma\gamma)/\Gamma(K_L \to \pi^0\pi^0\pi^0)$ with a statistical accuracy of 0.76% and a systematic accuracy of 0.86 % has been performed, based on a luminosity of 362 pb^{-1} integrated by KLOE in the years 2001 and 2002. The accuracy on the ratio is determined by the accuracy in the measurement of the rarest channel $K_L \to \gamma\gamma$: the statistical error is dominated by the event yield, the systematic one is given by the evaluation of selection efficiencies and background subtraction. A statistical error of 0.77% has been reached using selection cuts with very high efficiency on the signal and high rejection power on the background. Control of the systematics arising from selection cuts has been done using subsamples of data with high purity. Systematics coming from background subtraction

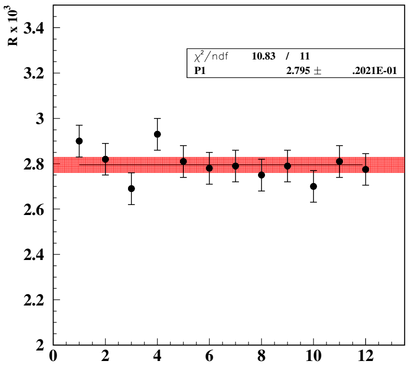

Figure 31: Value of $\Gamma(K_L \to \gamma\gamma)/\Gamma(K_L \to \pi^0\pi^0\pi^0)$ for subsamples of ~ 30 pb^{-1} each.

has been studied by varying the shape of the background distribution in the signal region and looking at the variation in the signal yield. The result, $R = (2.79 \pm 0.02 \pm 0.02) \cdot 10^{-3}$, is in good agreement with the recent measurement from NA48, $R = (2.81 \pm 0.01 \pm 0.02) \cdot 10^{-3}$ [2]. Using the branching ratio for $K_L \to \pi^0\pi^0\pi^0$ [1], $(21.08 \pm 0.27)\%$, we obtain $BR(K_L \to \gamma\gamma) = (5.89 \pm 0.07 \pm 0.08) \times 10^{-4}$ where the second is the systematic error due to the knowledge of $BR(K_L \to \pi^0\pi^0\pi^0)$.

8 Acknowledgements

We want to warmly acknowledge Doct. C. Bloise and Prof. F. Ceradini for many useful discussions, precious suggestions and constant encouragement during the whole work.

References

[1] K.Hagiwara et al., Physical Review D66 (2002) 010001-1

[2] A.Lai et al., *Precise measurement of the $K_S \to \gamma\gamma$ and $K_L \to \gamma\gamma$ decay rates*, Phys. Lett. B551 (2003), 7.

[3] S.Di Falco and A.Giannasi, *Study of the $BR(K_L \to \gamma\gamma)/BR(K_L \to \pi^0\pi^0\pi^0)$*, KLOE memo n.259, November 2001

[4] S.Di Falco, *The K_L tagging algorithm*, KLOE memo n.173, February 1998

[5] S.Miscetti and T.Spadaro *Rate measurement of accidental clusters in the EMC* , KLOE memo n.251, October 2001.

[6] M.Adinolfi et al., Nuclear Instruments and Methods A492 (2002) 134